28 THz soliton frequency comb in a continuous-wave pumped fiber Fabry-Pérot resonator

T. Bunel, M. Conforti, Z. Ziani, Julien Lumeau, A. Moreau, A. Fernandez, O. Llopis, G. Bourcier, A. Mussot

28 THz soliton frequency comb in a continuous-wave pumped fiber Fabry-Pérot resonator

T. Bunel,[1] M. Conforti,[1] Z. Ziani,[1] J. Lumeau,[2] A. Moreau,[2] A. Fernandez,[3] O. Llopis,[3] G. Bourcier,[3, a)] and A. Mussot[1]

[1)] *University of Lille, CNRS, UMR 8523-PhLAM Physique des Lasers, Atomes et Molécules, F-59000, Lille, France*

[2)] *Aix Marseille University, CNRS, Centrale Marseille, Institut Fresnel, Marseille, France*

[3)] *LAAS-CNRS, Université de Toulouse, CNRS, 7 avenue de Colonel Roche, 31031 Toulouse, France*

(*Electronic mail: thomas.bunel@univ-lille.fr)

(Dated: 8 September 2023)

We report the generation of an optical frequency comb featuring 28 THz bandwidth, sustained by a single 80 fs cavity soliton recirculating in a fiber Fabry-Pérot resonator. This large spectrum is comparable to frequency combs obtained with microresonators operating in the anomalous dispersion regime. Thanks to the compact design and the easy coupling of the resonator, cavity solitons can be generated in an all-fiber experimental setup with a continuous wave pumping scheme at moderate pump powers. We also observe the generation of a dispersive wave at higher frequencies which is supported by higher-order dispersion. These observations align remarkably well with both numerical simulations and the established theory of cavity solitons.

I. INTRODUCTION

Nonlinear Kerr cavities have enabled the generation of cavity solitons (CSs)[1–5], which offer precise femtosecond sources and wide-ranging optical frequency combs (OFCs) with repetition rates spanning from MHz to THz, impacting a wide range of cross-disciplinary applications: data transmission[6] and processing[7], ranging[8], microwave photonics[9], dual-comb spectroscopy[10], and astronomical spectrograph calibration[11]. These solitons arise as localised solutions of the Lugiato–Lefever equation[12,13] (LLE) and can be observed in resonators with high-quality factors. The emergence of CSs relies on the double balance between anomalous group velocity dispersion (GVD) and Kerr nonlinearity on one side, and between losses and energy injection (typically achieved through continuous-wave (CW) laser pumping) on the other side. Owing to their high-quality factor and compact design (cavity length of hundreds of microns), microresonators have attracted significant attention over the last decade[4,5,14]. Despite these impressive performances, launching and collecting light in these resonators can be challenging, requiring advanced fiber coupling devices such as a prism fiber taper[15] or advanced coupling methods for chip microresonators[16], and while progresses on packaging are on going, it is still an obstacle for fiber applications. Another way to generate OFCs in resonators consists in using all-fiber ring cavities of tens of meters in length[1,17], whose effective quality factor can reach several millions by including an amplifier within the cavity[18]. Spectra obtained using these resonators architecture extend over several THz, almost like microresonators, but they have two major drawbacks. Firstly, the line spacing is in the MHz range, which limits the field of application (mostly in the GHz range[14]), and secondly, they are not compact. An interesting alternative consists in taking benefit of fiber Fabry–Pérot (FFP) resonators of several centimeters in length. They are a good compromise between fiber ring cavities and microresonators, offering several tens of millions of Q-factors, as well as easy connection to photonic devices with a standard physical-contact fiber connector (FC/PC) and small size[3,19–23]. CS generation has already been demonstrated with these devices using either a pulsed pumping scheme[3] or stabilization management through the Brillouin effect[19,24]. These recent studies have paved the way for this novel method of OFC generation. However, the generated CSs via CW pumping still have durations exceeding 200 fs[19,24], which falls short of the performance achieved by microresonators.

This study demonstrates that manufacturing a FFP resonator using a highly nonlinear fiber with low GVD at the pump wavelength enables the generation of sub-100 fs CSs. Moreover, we implemented an advanced triggering experimental setup enabling an accurate and easy control of the detuning to explore the different regimes of the cavity before reaching the soliton states together with an efficient stabilization feature. Additionally, the inherent low GVD characteristics, combined with the large spanning of the generated CS, leads to the emergence of dispersive radiation due to higher-order dispersion, which permits to observe a broad spectrum spanning over 28 THz.

II. FABRICATION OF THE CAVITY

The FFP cavity used for the study is depicted in Fig. 1. It is made from an optical highly nonlinear fiber (HNLF) of length L = 20.63 cm, a group velocity dispersion (GVD) of $\beta_2 = -0.8$ ps^{2}km^{-1}, a third-order dispersion (TOD) of $\beta_3 = 0.03$ ps^{3}km^{-1} at the pump wavelength (1550 nm) and a nonlinear coefficient of $\gamma = 10.8$ W^{-1}km-1. Both fiber ends are mounted in FCs/PC, and Bragg mirrors are deposited at each extremity with a physical vapor deposition technique,

[a)] Also at CNES, 18 Avenue Edouard Belin, F-31401 Toulouse, France

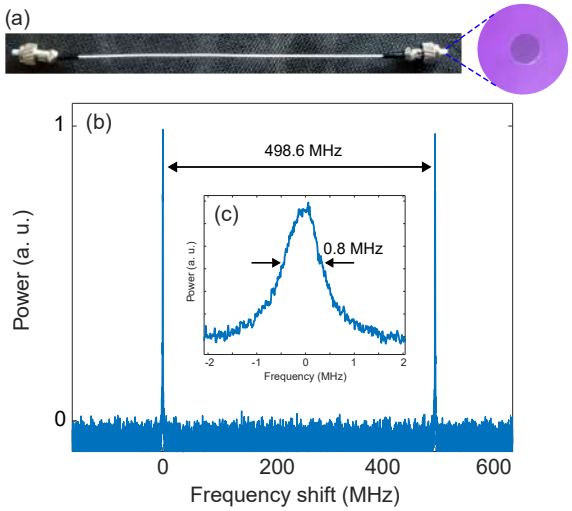

FIG. 1. Description of the FFP resonator. (a) Photograph of device with one of its deposited mirror. (b) Transmission function of resonator in linear regime. (c) Zoom on a cavity resonance

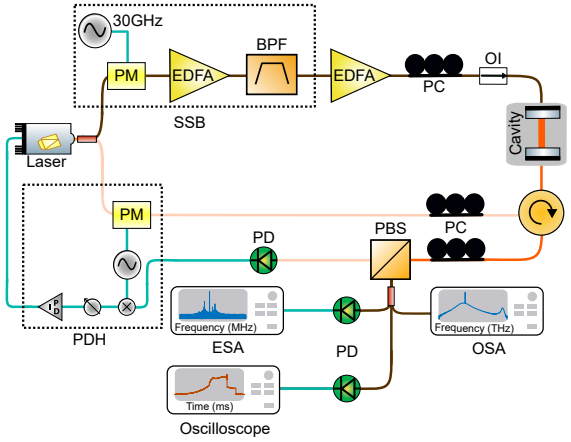

FIG. 2. Experimental setup with a two-arms stabilization system. Brown line: pumping path; beige line: stabilization path. The pumping and stabilization beams are perpendicularly polarized to each other. PM: Phase Modulator; EDFA: Erbium Doped Fiber Amplifier; PC: Polarization Controller; OI: Optical Isolator; PD: Photodiode; PDH: Pound-Drever-Hall; SSB: single-side-band generator.

to achieve 99.86% reflectance over a 100 nm bandwidth[25]. Fig. 1(a) shows a connector with its deposited mirror. The linear transfer function is shown in Figs. 1(b) and (c). This architecture leads to a resonator with a sub-MHz linewidth resonance, and a free spectral range (FSR) equal to 498.6 MHz, corresponding to a finesse $\mathscr{F} = 620$, and a quality-factor $Q = 230 \cdot 10^6$. One of the great advantages of this FFP with respect to a microresonator[15,16] is its plug-and-play feature into an all-fiber photonic device.

III. EXPERIMENTAL SETUP

The FFP resonator is exploited in the experimental setup described in Fig 2. The generation of CSs requires bistable operation and specific excitation protocols[5,14]. One of the most popular and efficient solution consists in performing a scan of the resonance from blue to red and to stop at a precise laser frequency, which fixes a specific cavity detuning. To achieve precise control over the cavity detuning, a two-arms stabilization scheme is implemented[22,26]. The CW laser is split into two beams: one beam serves as the control beam for stabilizing the laser on a cavity resonance (control beam), while the other beam acts as the pump beam for the cavity (nonlinear beam). The polarization states of the control and nonlinear beams are crossed in order to minimise nonlinear interactions between them. The polarisation states are adjusted using polarization controllers to ensure their separation at the output using a polarization beam splitter. This configuration allows independent handling of the beams and prevents their interaction within the cavity. The stabilization process [lower beige arm in the Fig. 2] is achieved through a Pound-Drever-Hall (PDH) system[27,28]. On the other hand, the detuning of the nonlinear beam [upper brown arm in Fig. 2], is controlled using a homemade tunable single-sideband generator [see SSB in Fig. 2]. The nearest side band of a modulated beam, obtained with a phase modulator driven by a 30 GHz tunable frequency synthesizer (TFS), is isolated to obtain a pump signal with a tunable frequency shift. The nonlinear beam is further amplified by an erbium-doped fiber amplifier to reach a power of 1 W before being launched into the cavity.

IV. CARACTERIZATION OF THE DIFFERENTS NONLINEAR REGIME OF THE CAVITY

Thanks to this setup, we can easily observe the distinct nonlinear regimes of the cavity, varying with the detuning, through the use of a basic CW pump. It is worth noting that the use of a PDH system for stabilization make the experimental setup very robust compare to the use of a simple Proportional-Integral-Derivative (PID) systems. It allows to compensate environmental vibrations and the thermal effect due to the strong CW laser pump[29]. First, a classic fast redshift scan is applied. The TFS frequency is sweeped from 30 GHz to 30,5 GHz with a speed of 2 GHz/s. The evolution of the output power through the scan is recorded thanks to a photodiode and an oscilloscope, and is represented in Fig. 3(a). As expected, we observe three different regions [(1), (2), (3) in Fig. 3(a)], corresponding to the different well-known comb structures in Kerr resonators, in sequence: modulation instability (MI), chaos and solitons[2,4,5,30,31]. Second, in a way to observe the evolution of these three nonlinear regime, we perform a slow redshift scan recording for each TFS frequency value, the optical spectrum and radio frequency (RF) beatnote centered at the first beatnote (498.6 MHz), of the generated signal, with an optical spectrum analyzer (OSA) and an electrical spectrum analyzer (ESA), respectively. Fig. 3(b) and (c) illustrate the evolution of the experimental generated signal as a function of the detuning, which can be obtained by the relation: $\Delta\delta = -\frac{4\pi nL}{c}\Delta\nu$, where $\Delta\delta$ and $\Delta\nu$ are the detuning variation and TFS frequency variation, respectively (c and n

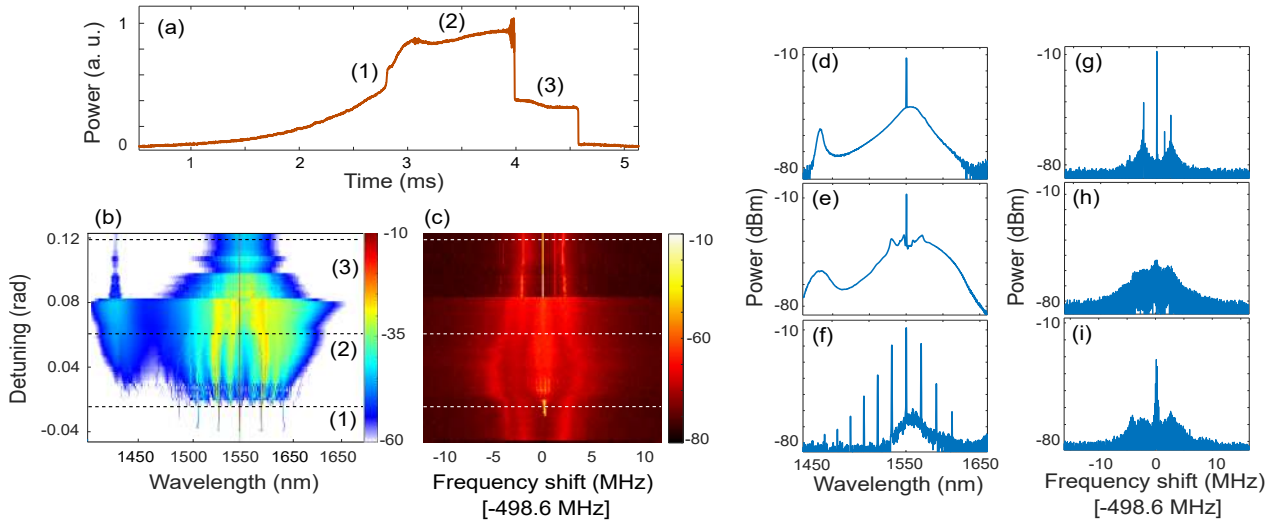

FIG. 3. Experimental recordings as a function of the cavity detuning. (a): Nonlinear transfer function with a fast redshift scan of the cavity (scan speed = 2 GHz/s). (b): Spectrum evolution with cavity detuning. (c): RF beatnote evolution with cavity detuning. (d), (e) and (f): Snapshot of each comb structure spectrum, corresponding to the black dashed lines in (b). (g), (h) and (i): Snapshot of each comb structure RF beatnote, corresponding to the white dashed lines in (c). (f) and (i): MI, $\delta = -0.015$ rad. (e) and (h): chaos, $\delta = 0.06$ rad. (d) and (g): soliton, $\delta = 0.12$ rad. The video in the supplemental material provides a comprehensive overview of the comb structure variation throughout the scan.

are speed of light in vacuum and the effective refractive index of the fiber mode) . In these figures, the three nonlinear regimes can easily be identified with a clear separation between each. Fig. 3(d)-(i) show several characteristic examples of the spectrum and RF beatnote of the three comb structures to get a clearer insight. (1) MI comb formation, characterized by its symmetric sidelobes around the pump in the spectral domain [Fig. 3(b) and (f)], resulting to a stable oscillation as the RF spectrum shows [Fig. 3(c) and (i)]. (2) MI lobe mixing leads to a chaotic transmission variation and produces a chaotic comb [Fig. 3(b) and (e)]. The chaotic regime is well illustrated by a huge broadening of the beatnote as showed in Fig. 3(c) and (h). The spectrum broadens, and a spectral component appears at 1430 nm due to the TOD as we will discuss below [Fig. 3(b) and (e)]. (3) CSs are generated resulting in a broad coherent optical OFC over 200 nm (i.e. 28 THz) [Fig. 3(d) and (g)]. Interestingly, Fig. 3(b) shows the existence of different CSs regime, indicating the circulation of multiple solitons within the cavity. However, the sensitivity the detection system in Fig. 3(a) does not allow to clearly highlight the different soliton regimes, from several CSs to a single one. The low sensitivity of the used photodiode might be the reason behind this discrepancy, as multiple steps may be present but not detectable.

In order to get a complete characterisation of the dynamics of the system, we record the phase noise spectra corresponding to each regime in Fig. 4: MI comb, multiple soliton comb, and single soliton comb. These measurements confirm that CSs present the most stable regimes. As expected, the phase noise of the MI comb is significantly higher (40 dB) compared to CSs. An interesting observation is that the phase noise of the multiple soliton comb closely resembles that of the single soliton comb in the low frequencies. However, in the high frequencies, the multiple soliton comb demonstrates considerably higher phase noise compared to the single soliton comb, 30 dB higher, with a comparative level to the MI comb.

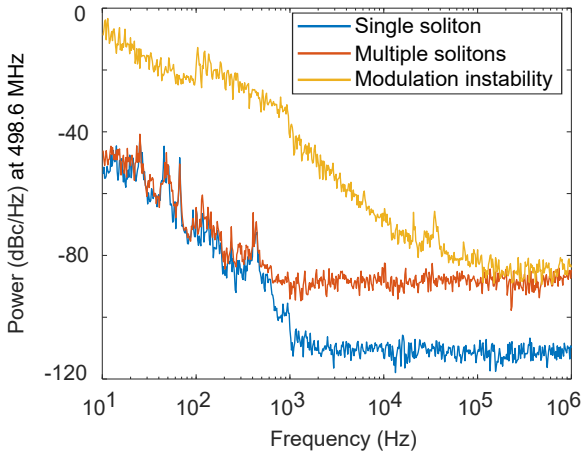

FIG. 4. Phase noise spectrum measurements of different generated signals. Modulation instability: $\delta = -0.015$ rad; multiple solitons: $\delta = 0.1$ rad; single soliton: $\delta = 0.12$ rad

V. NUMERICAL SIMULATIONS

We reproduced the experimental results by numerically solving the Lugiato-Lefever equation adapted for FFP cavi-

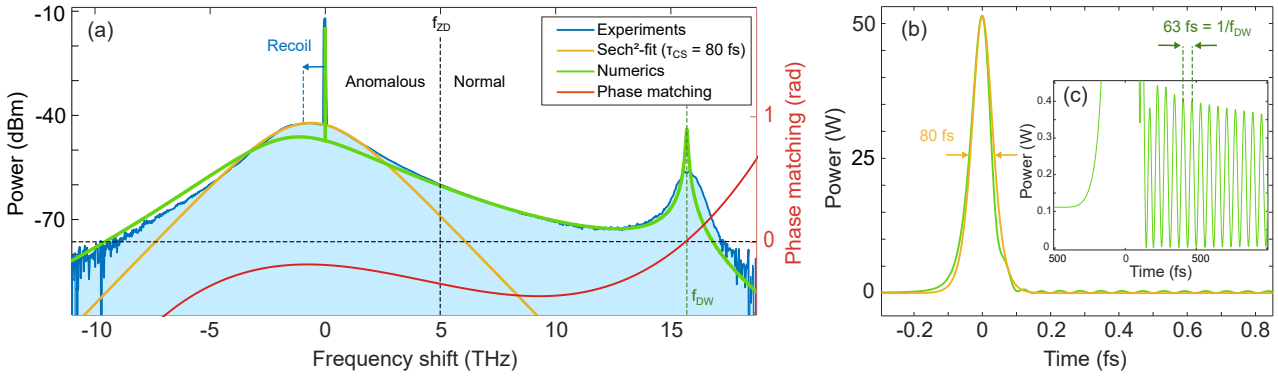

FIG. 5. Cavity soliton in higly nonlinear FFP resonator. (a) Spectral domain. (b) Time domain. Blue line: experiment; green line: simulation; orange line: sech² curve fit; red line: phase matching curve. f_{ZD} indicates the frequency of the zero-dispersion and f_{DW} indicates the frequency of the DW.

ties (FPLLE)[3,32,33]:

$$t_R\frac{\partial\psi}{\partial\tau} = -(\alpha+\delta)\psi+\theta\sqrt{P_{in}} + 2L\left[-i\frac{\beta_2}{2}\frac{\partial^2}{\partial t^2}+i\gamma|\psi|^2+i\gamma\frac{2}{t_R}\int_{-t_R/2}^{t_R/2}|\psi|^2dt\right]\psi, \quad (1)$$

where P_{in} is the input power, $t_R = 1/FSR(=2.0056ns)$ is the roundrip time, $\theta = 0.0529$ is the transmissivity of the mirror and $\alpha = \pi/\mathscr{F}$ accounts for the total cavity losses (valid for $\mathscr{F} \gg 1$). We used the same parameters as in experiments and set the detuning to $\delta = 0.12$. Fig. 5(a) shows the measured soliton spectrum, spanning over an impressive 28 THz. The experimental spectrum is in good agreement with the numerical predictions obtained by FPLLE, represented in green in Fig. 5(a). As for microresonators[34], the use of a fiber with low GVD and a high nonlinear coefficient enables the generation of broader spectra, compared to those achieved with conventional telecom fibers[3,24], even with moderate pump power. Note that the SMF-HNLF transition induce 3 dB losses, i.e. an effective input power $P_{in} = 0.5$ W. The simulation reveals the generation of a soliton of 80 fs duration [green line in Fig. 5(b)], which agrees with the sech²-envelope fit [yellow lines in Fig. 5(a) and (b)].

In addition, an important spectral peak 15 THz away from the pump is observed. This corresponds to a dispersive wave (DW), also known as Cherenkov radiation, which is emitted by the CS due to high-order dispersion (HOD)[17,35–39]. Indeed, the cavity is pumped only 5 THz away from the zero-dispersion wavelength (ZDW), allowing an efficient radiation process. The frequency of the DW with respect to the soliton satisfies the phase matching condition[17,35,37] reported in Eq. (2):

$$\frac{2L\beta_3}{3!}\omega^3+\frac{2L\beta_2}{2!}\omega^2-D\omega-\delta=0. \quad (2)$$

Here, ω is the normalized angular frequency shift of the driving field, and D represents the group-delay accumulated by the temporal CSs with respect to the driving field over one round trip (in units of time). Indeed, TOD makes the CSs group-velocity slightly different from that of the driving field, leading to a spectral recoil[17,37]. This phenomenon is observable in both the experimental and simulated spectra presented in Fig. 5(a). Thus, the soliton propagates together with the extended radiation tail attached to it [green line in Fig. 5(b) and (c)]. The measured DW frequency position (15.77 THz) is almost identical to the one derived from the phase matching condition (15.69 THz) [red line in Fig. 5(a)], itself identical to the frequency position of the simulated DW [green line in Fig. 5(a)]. The drift delay is calculated as $D = \beta_2\Omega_{CS}2L+\beta_3\Omega_{CS}^2L$, where the recoil frequency shift $\Omega_{CS}/(2\pi) = 1105$ GHz is determined through the numerical simulation [green line in Fig. 5(a)] as in Ref.[17]. It is worth noting that the nonlinear contribution, which depends on the cavity length and CS background power, is not incorporated in the phase matching condition, due to its negligible impact. Nevertheless, it becomes relevant in specific studies, such as Ref.[17]. In the context of FFP cavities, accounting for this would entail considering the specific characteristics of the two-way light circulation, and the additional phase arising from cross-phase modulation[32,33,40]. However, this aspect falls outside the scope of this study but presents a potential avenue for exploration in subsequent investigations involving adapted cavities.

VI. CONCLUSION

In this study, we have reported the generation of an OFC spanning over 28 THz (i.e. 200 nm), corresponding to a 80 fs cavity soliton duration emitting a dispersive wave, by using a high-quality factor FFP resonator pumped by a CW laser. The use of this kind of cavity benefits of the ease of implementation into photonic systems by means of its FC/PC connectors. Moreover, our advanced setup with an independent control of the cavity detuning and of the stabilization beam, enabled a smooth tuning of the cavity detuning to observe the dynamics of the system, as well as an excellent stabilization of the cavity with a PDH system to reach -110 dBc/Hz in the best case. The overlap of the CS with the normal dispersion lead to the generation of a DW at 15 THz from the pump. These experimental results are in excellent agreement with numerical simulations. This work contribute to the development of new

platforms to generate OFCs, with a view of new applications for fiber systems.

ACKNOWLEDGMENTS

We are grateful to Nicolas Englebert for fruitful discussions.

The present research was supported by the agence Nationale de la Recherche (Programme Investissements d'Avenir, I-SITE VERIFICO); Ministry of Higher Education and Research; European Regional Development Fund (Photonics for Society P4S), the CNRS (IRP LAFONI); Hauts de France Council (GPEG project); A.N.R. ASTRID ROLLMOPS; and the university of Lille (LAI HOLISTIC)

DATA AVAILABILITY STATEMENT

The data that support the findings of this study are available from the corresponding author upon reasonable request.

REFERENCES

[1]F. Leo, S. Coen, P. Kockaert, S.-P. Gorza, P. Emplit, and M. Haelterman, "Temporal cavity solitons in one-dimensional kerr media as bits in an all-optical buffer," Nature Photonics **4**, 471–476 (2010).

[2]T. Herr, V. Brasch, J. D. Jost, C. Y. Wang, N. M. Kondratiev, M. L. Gorodetsky, and T. J. Kippenberg, "Temporal solitons in optical microresonators," Nature Photonics **8**, 145–152 (2014).

[3]E. Obrzud, S. Lecomte, and T. Herr, "Temporal solitons in microresonators driven by optical pulses," Nature Photonics **11**, 600–607 (2017).

[4]T. J. Kippenberg, A. L. Gaeta, M. Lipson, and M. L. Gorodetsky, "Dissipative Kerr solitons in optical microresonators," Science **361**, eaan8083 (2018).

[5]A. Pasquazi, M. Peccianti, L. Razzari, D. J. Moss, S. Coen, M. Erkintalo, Y. K. Chembo, T. Hansson, S. Wabnitz, P. Del'Haye, X. Xue, A. M. Weiner, and R. Morandotti, "Micro-combs: A novel generation of optical sources," Physics Reports **729**, 1–81 (2018).

[6]P. Marin-Palomo, J. N. Kemal, M. Karpov, A. Kordts, J. Pfeifle, M. H. P. Pfeiffer, P. Trocha, S. Wolf, V. Brasch, M. H. Anderson, R. Rosenberger, K. Vijayan, W. Freude, T. J. Kippenberg, and C. Koos, "Microresonator-based solitons for massively parallel coherent optical communications," Nature **546**, 274–279 (2017).

[7]M. Tan, X. Xu, J. Wu, R. Morandotti, A. Mitchell, and D. J. Moss, "RF and microwave photonic temporal signal processing with Kerr micro-combs," Advances in Physics: X **6**, 1838946 (2021).

[8]P. Trocha, M. Karpov, D. Ganin, M. H. P. Pfeiffer, A. Kordts, S. Wolf, J. Krockenberger, P. Marin-Palomo, C. Weimann, S. Randel, W. Freude, T. J. Kippenberg, and C. Koos, "Ultrafast optical ranging using microresonator soliton frequency combs," Science **359**, 887–891 (2018).

[9]E. Lucas, P. Brochard, R. Bouchand, S. Schilt, T. Südmeyer, and T. J. Kippenberg, "Ultralow-noise photonic microwave synthesis using a soliton microcomb-based transfer oscillator," Nature Communications **11**, 374 (2020).

[10]M.-G. Suh, Q.-F. Yang, K. Y. Yang, X. Yi, and K. J. Vahala, "Microresonator soliton dual-comb spectroscopy," Science **354**, 600–603 (2016).

[11]E. Obrzud, M. Rainer, A. Harutyunyan, M. H. Anderson, J. Liu, M. Geiselmann, B. Chazelas, S. Kundermann, S. Lecomte, M. Cecconi, A. Ghedina, E. Molinari, F. Pepe, F. Wildi, F. Bouchy, T. J. Kippenberg, and T. Herr, "A microphotonic astrocomb," Nature Photonics **13**, 31–35 (2019).

[12]L. A. Lugiato and R. Lefever, "Spatial dissipative structures in passive optical systems," Physical Review Letters **58**, 2209–2211 (1987).

[13]M. Haelterman, S. Trillo, and S. Wabnitz, "Additive-modulation-instability ring laser in the normal dispersion regime of a fiber." Optics letters **17**, 745–747 (1992).

[14]Y. Sun, J. Wu, M. Tan, X. Xu, Y. Li, R. Morandotti, A. Mitchell, and D. J. Moss, "Applications of optical microcombs," Advances in Optics and Photonics **15**, 86 (2023).

[15]M. Cai, O. Painter, and K. J. Vahala, "Observation of Critical Coupling in a Fiber Taper to a Silica-Microsphere Whispering-Gallery Mode System," Physical Review Letters **85**, 74–77 (2000).

[16]L. Razzari, D. Duchesne, M. Ferrera, R. Morandotti, S. Chu, B. E. Little, and D. J. Moss, "CMOS-compatible integrated optical hyper-parametric oscillator," Nature Photonics **4**, 41–45 (2010).

[17]J. K. Jang, M. Erkintalo, S. G. Murdoch, and S. Coen, "Observation of dispersive wave emission by temporal cavity solitons," Optics Letters **39**, 5503 (2014).

[18]N. Englebert, C. Mas Arabí, P. Parra-Rivas, S.-P. Gorza, and F. Leo, "Temporal solitons in a coherently driven active resonator," Nature Photonics **15**, 536–541 (2021).

[19]K. Jia, X. Wang, D. Kwon, J. Wang, E. Tsao, H. Liu, X. Ni, J. Guo, M. Yang, X. Jiang, J. Kim, S.-n. Zhu, Z. Xie, and S.-W. Huang, "Photonic Flywheel in a Monolithic Fiber Resonator," Physical Review Letters **125**, 143902 (2020).

[20]Z. Xiao, T. Li, M. Cai, H. Zhang, Y. Huang, C. Li, B. Yao, K. Wu, and J. Chen, "Near-zero-dispersion soliton and broadband modulational instability Kerr microcombs in anomalous dispersion," Light: Science & Applications **12**, 33 (2023).

[21]T. Bunel, M. Conforti, Z. Ziani, J. Lumeau, A. Moreau, A. Fernandez, O. Llopis, J. Roul, A. M. Perego, K. K. Wong, *et al.*, "Observation of modulation instability kerr frequency combs in a fiber fabry–pérot resonator," Optics Letters **48**, 275–278 (2023).

[22]Z. Li, Y. Xu, S. Shamailov, X. Wen, W. Wang, X. Wei, Z. Yang, S. Coen, S. G. Murdoch, and M. Erkintalo, "Ultrashort dissipative Raman solitons in Kerr resonators driven with phase-coherent optical pulses," (2022), arXiv:2212.08223 [nlin, physics:physics], 2212.08223.

[23]T. Bunel, M. Conforti, J. Lumeau, A. Moreau, A. Fernandez, O. Llopis, J. Roul, A. M. Perego, and A. Mussot, "Unexpected phase-locked brillouin kerr frequency comb in fiber fabry perot resonators," (CLEO®/Europe 2023 - Postdeadline session, 2023).

[24]M. Nie, K. Jia, Y. Xie, S. Zhu, Z. Xie, and S.-W. Huang, "Synthesized spatiotemporal mode-locking and photonic flywheel in multimode mesoresonators," Nature Communications **13**, 6395 (2022).

[25]J. Zideluns, F. Lemarchand, D. Arhilger, H. Hagedorn, and J. Lumeau, "Automated optical monitoring wavelength selection for thin-film filters," Optics Express **29**, 33398 (2021).

[26]K. Nishimoto, K. Minoshima, T. Yasui, and N. Kuse, "Thermal control of a Kerr microresonator soliton comb via an optical sideband," Optics Letters **47**, 281 (2022).

[27]R. W. P. Drever, J. L. Hall, F. V. Kowalski, J. Hough, G. M. Ford, A. J. Munley, and H. Ward, "Laser phase and frequency stabilization using an optical resonator," Applied Physics B Photophysics and Laser Chemistry **31**, 97–105 (1983).

[28]E. D. Black, "An introduction to Pound–Drever–Hall laser frequency stabilization," American Journal of Physics **69**, 79–87 (2001).

[29]S. Zhang, J. M. Silver, L. Del Bino, F. Copie, M. T. M. Woodley, G. N. Ghalanos, A. Ø. Svela, N. Moroney, and P. Del'Haye, "Sub-milliwatt-level microresonator solitons with extended access range using an auxiliary laser," Optica **6**, 206 (2019).

[30]S. Coen and M. Erkintalo, "Universal scaling laws of Kerr frequency combs," Optics Letters **38**, 1790 (2013).

[31]P. Parra-Rivas, D. Gomila, M. A. Matías, S. Coen, and L. Gelens, "Dynamics of localized and patterned structures in the Lugiato-Lefever equation determine the stability and shape of optical frequency combs," Physical Review A **89**, 043813 (2014).

[32]Z. Ziani, T. Bunel, A. M. Perego, A. Mussot, and M. Conforti, "Theory of modulation instability in Kerr Fabry-Perot resonators beyond the mean field limit," (2023), arXiv:2307.13488 [nlin, physics:physics].

[33]D. C. Cole, A. Gatti, S. B. Papp, F. Prati, and L. Lugiato, "Theory of kerr frequency combs in fabry-perot resonators," Physical Review A **98**, 013831 (2018).

[34]X. Yi, Q.-F. Yang, K. Y. Yang, M.-G. Suh, and K. Vahala, "Soliton frequency comb at microwave rates in a high-Q silica microresonator," Optica **2**, 1078 (2015).
[35]M. Conforti and S. Trillo, "Dispersive wave emission from wave breaking," Optics Letters **38**, 3815 (2013).
[36]M. Erkintalo, Y. Q. Xu, S. G. Murdoch, J. M. Dudley, and G. Genty, "Cascaded Phase Matching and Nonlinear Symmetry Breaking in Fiber Frequency Combs," Physical Review Letters **109**, 223904 (2012).
[37]C. Milián and D. Skryabin, "Soliton families and resonant radiation in a micro-ring resonator near zero group-velocity dispersion," Optics Express **22**, 3732 (2014).
[38]V. Brasch, M. Geiselmann, T. Herr, G. Lihachev, M. H. P. Pfeiffer, M. L. Gorodetsky, and T. J. Kippenberg, "Photonic chip–based optical frequency comb using soliton Cherenkov radiation," Science **351**, 357–360 (2016).
[39]T. Wildi, M. A. Gaafar, T. Voumard, M. Ludwig, and T. Herr, "Dissipative Kerr solitons in integrated Fabry–Perot microresonators," Optica **10**, 650 (2023).
[40]W. J. Firth, J. B. Geddes, N. J. Karst, and G.-L. Oppo, "Analytic instability thresholds in folded kerr resonators of arbitrary finesse," Physical Review A **103**, 023510 (2021).